RAA 2020 Vol. **20** No. **8**, 131(11pp) doi: 10.1088/1674–4527/20/8/131

http://www.raa-journal.org *http://iopscience.iop.org/raa*

***R**esearch in*
***A**stronomy and*
***A**strophysics*

NLTE analysis of high-resolution *H*-band spectra IV: neutral copper

Xiao-Dong Xu, Jian-Rong Shi, Jun-Bo Zhang and Ze-Ming Zhou

Key Laboratory of Optical Astronomy, National Astronomical Observatories, Chinese Academy of Sciences, Beijing 100101, China; *sjr@bao.ac.cn*
School of Astronomy and Space Science, University of Chinese Academy of Sciences, Beijing 100049, China

Received 2020 January 31; accepted 2020 March 16

Abstract To obtain reliable Cu abundances with the APOGEE *H*-band spectra, it is important to investigate the non-local thermodynamic equilibrium (NLTE) effects on the formation of the *H*-band Cu I lines. In addition, the Cu atomic model needs to be tested. Based on both the high-resolution and high signal-to-noise ratio *H*-band spectra from the Apache Point Observatory Galactic Evolution Experiment (APOGEE) and optical data, we derived the LTE and NLTE copper abundances of 13 FGK sample stars with the spectral synthesis method. We find that the NLTE effects are negligible for the Cu I 16005.7Å line in the IR *H*-band. Consistent copper abundances within the uncertainties from these two sets of lines have been obtained, which indicates the reliability of our NLTE copper atomic model. We note that the [Cu/Fe] ratios increase with increasing metallicity when $\sim$ –1.4 dex $<$ [Fe/H] $<\sim$ –0.5 dex, favoring a secondary (metallicity-dependent) copper production.

Key words: line: formation — line: profiles — stars: abundances — stars: atmospheres

1 INTRODUCTION

Different elemental abundance trends provide important information to trace their astrophysical formation and they can help to constrain the Galactic theoretical evolutionary models. Copper is of particular interest because it can be synthesized through several nucleosynthetic processes (Bisterzo et al. 2004): *a*) slow neutron capture (*s*-process), either main (i.e., taking place in low- and intermediate-mass asymptotic giant branch stars, Arlandini et al. 1999) or weak (i.e., occurring in massive stars during core-helium, carbon-shell and the explosive complete Ne burning stages, Woosley & Weaver 1995; Limongi & Chieffi 2003; Pignatari et al. 2010); *b*) the explosive nucleosynthesis, either in SNe II (Timmes et al. 1995) or long-lived SNe Ia (Matteucci et al. 1993; Iwamoto et al. 1999; Travaglio et al. 2004; Fink et al. 2014); *c*) the *weak sr*-process.

The respective importance of the miscellaneous processes is still under debate. Matteucci et al. (1993) suggested that the main source of copper was SNe Ia, which was subsequently supported by the studies of Mishenina et al. (2002) and Simmerer et al. (2003). Meanwhile, Bisterzo et al. (2004) claimed that most solar Cu was synthesized by the *weak sr*-process in massive stars and there was no need for an extra contribution by SNe Ia. Predictions of Galactic chemical evolution (GCE) model of Romano & Matteucci (2007) and Romano et al. (2010) also supported massive stars played a dominant role in copper production. Therefore, detailed and reliable [Cu/Fe] trend is essential to figure out these problems.

Many groups have studied copper abundances for various samples, covering a wide range of metallicity from extreme metal-poor stars to solar ones. Generally, the Galactic disk/halo [Cu/Fe] trend can be represented for low metallicity stars up to [Fe/H] ≈ -1.5 dex by a flat distribution around [Cu/Fe] $\approx$ –0.7 to –1.0 dex (e.g., Westin et al. 2000; Cowan et al. 2002; Sneden et al. 2003; Bihain et al. 2004; Lai et al. 2008) followed by a linear increase with a slope close to 1 in the metallicity range –1.5 dex $<$ [Fe/H] $<$ –0.7 dex (e.g. Gratton & Sneden 1988; Sneden & Crocker 1988; Sneden et al. 1991; Mishenina et al. 2002; Simmerer et al. 2003; Yan et al. 2015, 2016). Then, it is roughly flat for stars of [Fe/H] from $\sim$–0.7 dex up to solar metallicity (e.g., Reddy et al. 2003, 2006; Ishigaki et al. 2013). But it should be noted that most of these analyses were carried out under local thermodynamic equilibrium (LTE) assumptions. NLTE effects play an important role in reliable Cu abundance calculations because they can affect the values as a

function of surface temperature, gravity, and/or metallicity of stars. Recently, several studies have derived NLTE copper abundances, which demonstrated that the NLTE effects were evident for Cu I lines, particularly for metal-poor stars (e.g., Yan et al. 2015, 2016; Shi et al. 2014, 2018; Andrievsky et al. 2018; Xu et al. 2019). Obviously, more work is needed to better investigate the [Cu/Fe] ratios with NLTE calculations.

The majority of the Cu measurements are based on the optical Cu I lines, sometimes on UV Cu lines. The exceptions are the measurements of Smith et al. (2013) and Hawkins et al. (2016), who used the Cu I lines in APOGEE IR *H*-band spectra and both of these two studies were performed in LTE conditions. The APOGEE survey aims to explore red giants across all components of the Milky Way and it has high resolution ($R \sim 22\,500$) and wide wavelength coverage of 1.51–1.70 μm spectra (e.g., Eisenstein et al. 2011; Majewski et al. 2017; Abolfathi et al. 2018). This has allowed us to get rid of the impact of extinction and better understand the chemical enrichment history of the whole Galaxy (including the Galactic disk, halo, and bulge). Although the APOGEE survey provides various elemental abundances, these values were calculated in LTE assumptions. Zhang et al. (2016, 2017) respectively determined the Si and Mg NLTE abundances of 13 disk stars with the APOGEE *H*-band spectra. Their results showed that the NLTE corrections were large and suggested that it was important to take the NLTE effects into account when deriving the [Si/Fe] and [Mg/Fe] ratios. While Zhou et al. (2019) analyzed the NLTE Ca abundances for a sample of stars using the APOGEE *H*-band data and found the NLTE corrections for the *H*-band Ca lines were small, within 0.03 dex. Given this situation, it is imperative to investigate the NLTE effects of the *H*-band Cu I lines and make more reliable copper abundance calculations for studying the chemical evolution of the Galaxy with the APOGEE data in future work.

In the present analysis, we derived the LTE and NLTE copper abundances for a sample of stars based on the APOGEE *H*-band and optical data with the spectral synthesis method. In Section 2, we briefly summarize the observations. Section 3 provides the adopted *H*-band and optical atomic line data, model atmospheres, and stellar parameters. Then, the copper atomic model and the NLTE effects are reported in Section 4. In Section 5, we present and discuss the results, including the derived copper abundances, abundance uncertainty, the comparisons and discussion, and the evolution trend of [Cu/Fe] in the Galactic disk. Finally, the conclusions are described in Section 6.

2 OBSERVATIONS

The stellar sample presented in this paper has been discussed in Zhang et al. (2016, 2017), which the reader is referred to for more details. Here, we briefly list the key points of the sample and the observations[1].

1. Our stellar sample represents the typical FGK stars with effective temperature ($T_{\rm eff}$) from about 4000 to 6500 K, surface gravity ($\log g$) from about 0.0 to 5.0 dex, and metallicity ([Fe/H]) from about –2.0 to 0.5 dex. Meanwhile, they have both the available high resolution ($R \gtrsim 20\,000$) and high signal-to-noise ratio (S/N $\gtrsim$ 100) optical and *H*-band spectra. The final sample stars have parameters in the ranges $4275 \leq T_{\rm eff} \leq 6070$ K, $1.67 \lesssim \log g \lesssim 4.65$ dex, and $-1.35 \lesssim$ [Fe/H] $\lesssim +0.28$ dex.
2. The *H*-band spectra used in this work were obtained from the SDSS IV/APOGEE2 survey DR14 (Abolfathi et al. 2018) and the spectra had been reduced and combined following Holtzman et al. (2015, 2018). The spectral normalization was carried out with our own code. The high-quality solar IR spectrum from the Kurucz's website[2] and Arcturus IR spectrum obtained from the National Optical Astronomy Observatory (NOAO) data archives[3] (more observational information can be seen in Hinkle et al. 1995) were also used in this work.
3. We adopted the optical solar spectrum from Kitt Peak Solar Atlas (Kurucz et al. 1984). For the other stars, the optical spectra were observed using several different telescopes, and their characteristics can be found in Zhou et al. (2019)(see their table 1). Overall, the optical spectra have a satisfactory resolving power of more than 50 000 and S/N $\geq$150.

3 METHOD OF CALCULATION

3.1 Atomic Line Data

3.1.1 Optical atomic line data

To acquire reliable abundances and better consistency, we selected four optical lines, which are relatively clean (minimizing the effects of nearby spectral features) and are available for all of our sample stars. Table 1 presents the main characteristics of the investigated optical atomic lines data. The oscillator strengths, $\log gf$,

[1] It was noted that we used the APOGEE DR14 spectra rather than DR12 (used in Zhang et al. 2016, 2017), because the DR12 release did not provide [Cu/Fe]. For better resolution and S/N, we used the optical spectra from Zhou et al. (2019).

[2] http://kurucz.harvard.edu

[3] http://ast.noao.edu/data/

Table 1 Atomic Data of the Copper Line

λ_{air} (Å)	Transition	$E_{\rm low}$ (eV)	$\log gf$	$\log C_6$
5105.541	$4s^2\ ^2D_{5/2} - 4p\ ^2P^o_{3/2}$	1.389	–1.64	–31.67
5218.202	$4p\ ^2P^o_{3/2} - 4d\ ^2D_{5/2}$	3.817	+0.28	–30.57
5700.240	$4s^2\ ^2D_{3/2} - 4p\ ^2P^o_{3/2}$	1.642	–2.60	–31.65
5782.132	$4s^2\ ^2D_{3/2} - 4p\ ^2P^o_{1/2}$	1.642	–1.89	–31.66
16005.748	$5s\ ^2S - 5p\ ^2P^o_{1/2}$	5.348	–0.018	–32.00

The $\log gf$ values were rectified by fitting the solar spectrum for the optical lines and by fitting the Arcturus IR spectrum from Hinkle et al. (1995) for the *H*-band line both under the NLTE assumptions. The van der Waals damping constant ($\log C_6$) values were calculated according to Anstee & O'Mara (1991, 1995) for the optical lines and obtained from the VALD website for the *H*-band line.

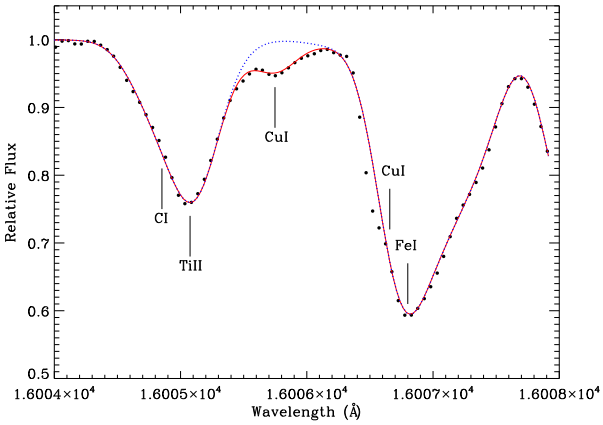

Fig. 1 Synthetic profiles of Cu I line at 16005.7 Å for the Arcturus IR spectrum from Hinkle et al. (1995). The *filled black circles* are the observation, the *red line* is the synthesis with Cu while the *dotted blue line* without the Cu line.

were rescaled with the absolute solar copper abundance of $\log \varepsilon_\odot$(Cu)= 4.25 dex (Asplund et al. 2009). The van der Waals damping constants, $\log C_6$, were calculated with Anstee & O'Mara (1991, 1995) tables. The ratio between the two copper isotopes (^{63}Cu and ^{65}Cu) was adopted as 0.69:0.31 (Asplund et al. 2009). The hyperfine structure (hfs) was also included in our analysis with the data taken from Biehl (1976).

3.1.2 IR H-band atomic line data

We noted that there are two copper lines in the APOGEE *H*-band spectra, the Cu I line at 16005.7 Å and the weak Cu I line at 16639.0 Å. Since the latter line is too weak to measure for our program stars, only the copper line at 16005.7 Å was analyzed in this study. As the Cu I line at 16005.7 Å is weak, and the uncertainty is large for the solar IR spectrum from the Kurucz's website, the $\log gf$ was rectified by fitting the Arcturus IR spectrum from Hinkle et al. (1995), which has high-resolution of 100 000 and high signal-to-noise ratio, with a given [Cu/Fe] (-0.13 dex) under the NLTE assumption. The [Cu/Fe] value for Arcturus was derived with the optical copper lines in Table A3 and is the mean NLTE result of the two optical Cu I lines. The absolute solar iron abundance of $\log \varepsilon_\odot$(Fe) = 7.45 dex (Asplund et al. 2009) was adopted to calculate the [Cu/Fe]. The fitting results are illustrated in Figure 1. It is noted that the $\log gf$ is similar to the value adopted by the Vienna Atomic Line Database (VALD), and our value is 0.027 dex higher. The van der Waals damping constant, $\log C_6$, was obtained from the VALD website[4]. As this Cu I line is weak and the effects of hfs will be negligible, we did not consider the hfs for it in our analysis.

In Figure 1, we show the synthetic profiles of the Cu I line at 16005.7 Å for the Arcturus. Although the copper *H*-band line is weak, it can be well reproduced and its line profile is clear and distinguishable from the adjacent lines (i.e., C I, Ti II and Fe I) at high-resolution. To avoid possible effects of the adjacent lines on our Cu abundances, we determined the C and Ti abundances of the Arcturus (given in Table A1) to obtain relatively reliable $\log gf$ values of these lines, and present the atomic data in Table A2.

[4] http://vald.inasan.ru/%7Evald3/php/vald.php

3.2 Model Atmospheres

In our analysis, the 1D LTE MARCS atmospheric models were adopted. As suggested by Gustafsson et al. (2008), for all of our program stars, the models were obtained by interpolation in the grid of spherical MARCS models for $-1.0\,{\rm dex} \leqslant \log g \leqslant 3.5\,{\rm dex}$. Meanwhile, they were calculated with plane-parallel symmetry for $3.5\,{\rm dex} \leqslant \log g \leqslant 5.5\,{\rm dex}$. For each individual model, the α-enhancement was included, as follows:

$$[\alpha/{\rm Fe}] = \begin{cases} 0.0 & \text{if} \quad 0.0 < [{\rm Fe/H}] \\ 0.4^*|[{\rm Fe/H}]| & \text{if} \quad -1.0 \leqslant [{\rm Fe/H}] \leqslant 0.0 \\ 0.4 & \text{if} \quad [{\rm Fe/H}] < -1.0 \end{cases}$$

3.3 Stellar Parameters

Reliable stellar parameters, effective temperature ($T_{\rm eff}$), surface gravity ($\log g$), metallicity ([Fe/H]) and microturbulence (ξ), are extremely important for abundance analyses. For this work, we employed stellar parameters of $T_{\rm eff} = 5777$ K, $\log g = 4.44$ dex, [Fe/H] = 0.0 dex, and $\xi = 0.90$ km s^{-1} for the Sun. For all of the other sample stars, we adopted the stellar parameters derived by Zhang et al. (2016). In their work, the effective temperature was determined by fulfilling the excitation equilibrium of Fe I, the surface gravity by forcing the ionization equi-

librium of Fe I and Fe II, and microturbulence by eliminating the [Fe/H] dependence of Fe I lines on their equivalent widths. The typical uncertainties of $T_{\rm eff}$, $\log g$, [Fe/H], and ξ are about $\pm$80 K, $\pm$0.1 dex, $\pm$0.08 dex, and 0.2 km s^{-1}. The final stellar parameters are presented in Table 2.

4 NLTE CALCULATION

4.1 Atomic Model

The copper atomic model adopted here was described in detail in Shi et al. (2014), which contained 97 energy levels (96 levels of Cu I and the ground state of Cu II) and 1089 transitions. The fine structure for low-excitation levels up to the $5p\,^2P^o$ term was also included. The photoionization cross sections and oscillator strengths, calculated by Liu et al. (2014) with the *R*-matrix method, were introduced into our atomic model. Both the inelastic collisions with hydrogen atoms and electrons for ionization and excitation were also included. The inelastic collisions with hydrogen atoms were obtained with Drawin's formula (Drawin 1968, 1969), which was described by Steenbock & Holweger (1984) with a scaling factor of $S_H = 0.1$ following the suggestion of Shi et al. (2014). Inelastic collisions with neutral hydrogen atoms will produce varying degrees of effects on the statistical equilibrium of Cu I in different stellar atmospheres. Shi et al. (2014, 2018) have done a series of test calculations for the Sun and a sample of metal-poor stars, and they found different Cu I lines will give consistent results for an investigated object when the $S_H = 0.1$ scale was adopted. Collisional excitations of allowed and forbidden transitions by electrons were calculated using the formulae of van Regemorter (1962) and Allen (1973), while collisional ionization rates were calculated with the formula of Seaton (1962).

To solve the coupled radiative transfer and statistical equilibrium equations, we adopted a revised DETAIL NLTEcode (Butler & Giddings 1985), which was based on an accelerated lambda iteration method (Rybicki & Hummer 1991, 1992), for the calculation of NLTE occupation numbers. Then, the synthetic line profiles were computed via the SIU program (Reetz 1991) using the departure coefficients from DETAIL.

4.2 NLTE Effects

The NLTE effects for optical copper lines have been investigated in detail by previous works (e.g., Shi et al. 2014, 2018; Yan et al. 2015, 2016; Andrievsky et al. 2018; Xu et al. 2019). As noted in these studies, the deviations from LTE are caused by the ultraviolet (UV) overionization in the deep atmosphere layers. In Figure 2, we plot the distribution of departure coefficients ($b_i = n_i^{\rm NLTE}/n_i^{\rm LTE}$) for the metal deficient star HD 58367. Here b_i is defined as the ratio of the number density of NLTE to that of LTE. For the sake of clarity, the approximate formation depths of the 5782 Å and 16005 Å lines are also presented in this figure, respectively. We can see that the number densities of the Cu II $3d\,^1S_0$ ground state becomes overpopulated in the upper atmosphere owing to overionization, and the Cu I ground state $4s\,^2S$ overlaps with the other two low excited levels $4s^2\,^2D_{5/2}$ and $4s^2\,^2D_{3/2}$. For the optical copper line at 5782 Å, we can see that the number densities of its lower ($4s^2\,^2D_{3/2}$) and upper ($4p\,^2P^o_{1/2}$) levels are underpopulated because of overionization for outside layers of $\log\,\tau_{5000} \lesssim 0.6$, and they are distinguishable even at the line formation region, which may result in large NLTE effects. While the line at 16005 Å forms in deep photospheric layers, which makes it rather weak. In this region, the populations of both the lower ($5s\,^2S$) and upper ($5p\,^2P^o_{1/2}$) terms of this transition depart from LTE to a low extent. Therefore, the NLTE effects of this line tend to be very small.

5 RESULTS AND DISCUSSION

5.1 Stellar Copper Abundances

For all of our program stars, the LTE and NLTE copper abundances were obtained through the spectral synthesis method. Abundances determination through this way was an iterative process and the Cu abundances varied until the differences between the synthetic spectra and the observed ones were minimized. During the fitting process, the broadenings caused by the instrument, rotation, and macroturbulence were treated as one single Gauss profile to be convolved with the synthetic flux profiles to fit the observed spectra. Moreover, the C and Ti abundances given in Table A1 were taken into account for our analysis to obtain reliable Cu abundances.

Figure 3 illustrates the observed and synthetic line profiles of two copper lines (an optical line at 5782 Å and an *H*-band line at 16005 Å) for HD 67447. It is obvious that the NLTE synthetic line profiles fit the observed spectra better than the LTE ones for the optical line at 5782 Å. As the copper line at 16005 Å is really weak (refer to Sect. 4.2), the differences between LTE and NLTE cannot be seen in this plot. In Table 2, we present the final copper abundances along with the standard deviation under LTE and NLTE assumptions. It can be found that the NLTE corrections are negligible for copper lines in the *H*-band, whereas they are evident with a variation from –0.02 to 0.10 dex for the optical lines. The LTE and NLTE Cu abundances derived from the individual optical lines are

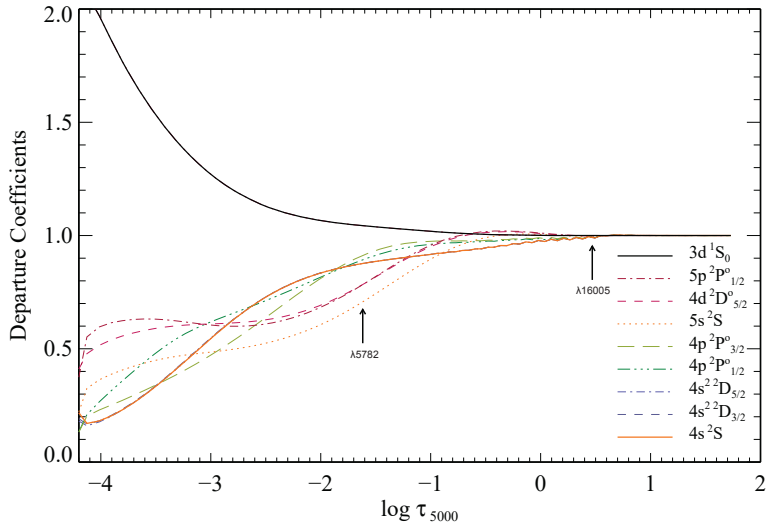

Fig. 2 Departure coefficients (b_i) for the important Cu I energy levels and the Cu II ground state as a function of continuum optical depth at 5000 Å for the model atmosphere of HD 58367.

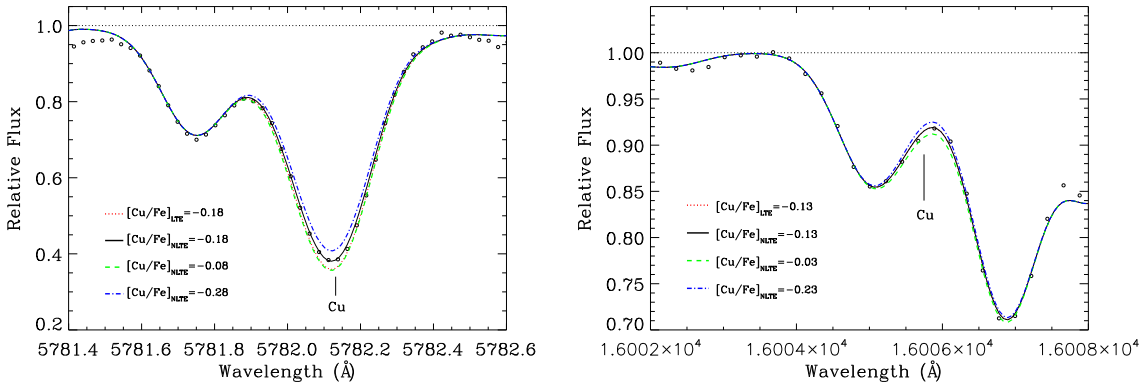

Fig. 3 Synthetic profiles of Cu I lines at 5782 Å and 16005 Å for HD 67447. The *open circles* are the observed spectra, the *black solid line* is the best-fitting synthesis (NLTE synthesis), the *red dotted curve* is the LTE profile with the same [Cu/Fe] relative to the NLTE, and the other two lines are NLTE synthetic spectra with [Cu/Fe] of ± 0.1 dex relative to the best fit.

Table 2 Stellar Copper Abundances

Star	$T_{\rm eff}$	log g	[Fe/H]	ξ	[Cu I$_{\rm LTE}$/Fe](ir)	[Cu I$_{\rm NLTE}$/Fe](ir)	$\Delta_{\rm ir}$	[Cu I$_{\rm LTE}$/Fe](opt)	[Cu I$_{\rm NLTE}$/Fe](opt)	$\Delta_{\rm opt}$	[Cu/Fe](ASPCAP)
Arcturus	4275	1.67	–0.58	1.60	–0.10	–0.10	0.00	–0.14 ± 0.01	–0.13 ± 0.03	0.01	–0.90 ± 0.06
HD 87	5053	2.71	–0.10	1.35	–0.12	–0.12	0.00	–0.23 ± 0.05	–0.21 ± 0.06	0.02	0.45 ± 0.03
HD 6582	5390	4.42	–0.81	0.90	–0.19	–0.19	0.00	–0.07 ± 0.04	–0.03 ± 0.07	0.04	–1.60 ± 0.28
HD 6920	5845	3.45	–0.06	1.40	–0.32	–0.32	0.00	–0.22 ± 0.05	–0.19 ± 0.06	0.03	–0.20 ± 0.06
HD 22675	4901	2.76	–0.05	1.30	–0.21	–0.21	0.00	–0.12 ± 0.02	–0.07 ± 0.03	0.05	0.37 ± 0.07
HD 31501	5320	4.45	–0.40	1.00	0.12	0.12	0.00	0.01 ± 0.01	0.02 ± 0.01	0.01	0.20 ± 0.05
HD 58367	4932	1.79	–0.18	2.00	–0.07	–0.07	0.00	–0.24 ± 0.04	–0.16 ± 0.05	0.08	0.73 ± 0.03
HD 67447	4933	2.17	–0.05	2.12	–0.13	–0.13	0.00	–0.26 ±0.01	–0.20 ± 0.02	0.06	0.75 ± 0.03
HD 102870	6070	4.08	0.20	1.20	–0.05	–0.05	0.00	–0.17 ± 0.03	–0.16 ± 0.04	0.01	0.12 ± 0.03
HD 103095	5085	4.65	–1.35	0.80	–0.20	–0.20	0.00	–0.35 ± 0.07	–0.31 ± 0.08	0.04	–2.20 ± 0.61
HD 121370	6020	3.80	0.28	1.40	0.00	0.00	0.00	–0.07 ± 0.02	–0.07 ± 0.02	0.00	0.25 ± 0.03
HD 148816	5830	4.10	–0.73	1.40	0.10	0.10	0.00	–0.10 ± 0.03	–0.02 ± 0.05	0.08	–0.63 ± 0.05
HD 177249	5273	2.66	0.03	1.65	–0.08	–0.08	0.00	–0.21 ± 0.03	–0.18 ± 0.05	0.03	0.59 ± 0.04

$\Delta_{\rm ir}$ and $\Delta_{\rm opt}$ stand for the NLTE effects (Δ =[Cu/Fe]$_{\rm NLTE}$ −[Cu/Fe]$_{\rm LTE}$) derived from the IR *H*-band and optical spectra, respectively.

Table 3 [Cu/Fe] Uncertainties Linked to Stellar Parameters

	ΔT 80 K	$\Delta \log g$ 0.1 dex	Δ[Fe/H] 0.08 dex	$\Delta\xi$ 0.2 km s^{-1}	$(\sum x^2)^{1/2}$
Δ[Cu/Fe](ir)	0.03	0.01	0.07	0.01	0.08
Δ[Cu/Fe](opt)	0.10	0.02	0.06	0.03	0.12

shown in Table A3. As indicated in this table, the NLTE effects differ from line to line even for the same stars.

5.2 Abundance Uncertainty

In Figure 3, we show the best-fitting NLTE synthesis using the black solid line for HD 67447, as well as the NLTE synthetic flux profiles with [Cu/Fe] of $\pm$ 0.1 dex relative to the best fit using the green and blue lines, respectively. It is clear that the variation of [Cu/Fe] can make a visible change of the NLTE synthesis. For our work, the synthetic flux profiles can be distinguished when the [Cu/Fe] changes about less than 0.1 dex. Considering the quality of our adopted spectra, the value of 0.1 dex can be our fit uncertainty to some extent. Meanwhile, the uncertainties on the derivation of copper abundances due to the choice of the stellar parameters should also be investigated. They are given in Table 3 for the star HD 67447 with the uncertainties of the stellar parameters described in Section 3.3. Assuming the errors are independent, the total uncertainties as the quadratic sum of all errors for the *H*-band and optical lines are listed in the last column.

5.3 Comparisons and Discussion

5.3.1 Comparison with the optical results and discussion

To verify our adopted copper atomic model, the differences between the Cu abundances derived from the APOGEE *H*-band data and those from optical spectra against the metallicity are presented in Figure 4. In this plot, open and filled circles respectively represent the differences under LTE and NLTE conditions. We note that the differences are $\lesssim$ 0.2 dex in LTE, while $\lesssim$ 0.15 dex in NLTE. Although NLTE reduces the scatter in the differences, the results still seem not so satisfactory, which can be explained by the uncertainties in the adopted atmospheric parameters and/or the continuum placement (see Sect.5.3.2). On the whole, we can state that the Cu abundances obtained from IR *H*-band and optical lines match roughly well, and our atomic model can be used to analyze the NLTE copper abundances.

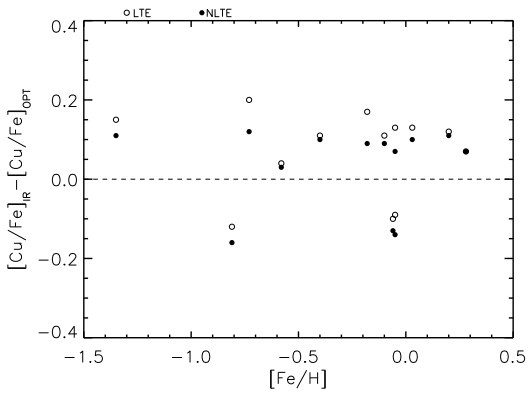

Fig. 4 Differences between the Cu abundances derived from the APOGEE *H*-band and optical spectra for our sample stars.

5.3.2 Comparison with the ASPCAP results and discussion

Abundances for up to 23 chemical elements are provided in the APOGEE DR14 release, and they are automatically derived by the APOGEE Stellar Parameters and Chemical Abundances Pipeline (ASPCAP) (Holtzman et al. 2015; García Pérez et al. 2016). The raw Cu abundance determinations are made for DR14, while no calibration results are presented due to the challenges of blends and they are not recommended to be used (Holtzman et al. 2018; Jönsson et al. 2018). Comparing the abundance derived by the ASPCAP with our independent analyses will enable a performance evaluation of the ASPCAP and probably calibrate its results.

The ASPCAP [Cu/Fe] ratios are given in the last column of Table 2. Through inspection of this table, a large discrepancy between these two works can be found, which can reach to as high as 1.98 dex for HD 103095. Figure 5 visually shows the differences between the ASPCAP and our results. Even though the exact causes of the discrepancy are unclear, we speculate that it may primarily result from the different continuum determination. As described in Section 4.2, the copper line in the APOGEE *H*-band spectra is very weak, thus the continuum placement requires great care, otherwise it can have a large effect on the final Cu abundances. For all of our sample stars, we tested to make a 1% shift of the continuum, and obtained the relative changes in Cu abundances. We find that this shift will yield a random variation of about 0.1 to 0.4 dex in the final [Cu/Fe] values. To intuitively present the effect, we randomly select a metal-poor star HD 67447 for discussion, and show its synthetic profiles in Figure 6.

Another possible reason for the discrepancy is due to the negligence of other lines blending. In Figure 7, we illustrate the synthetic profiles of Cu I line at 16005.7 Å for

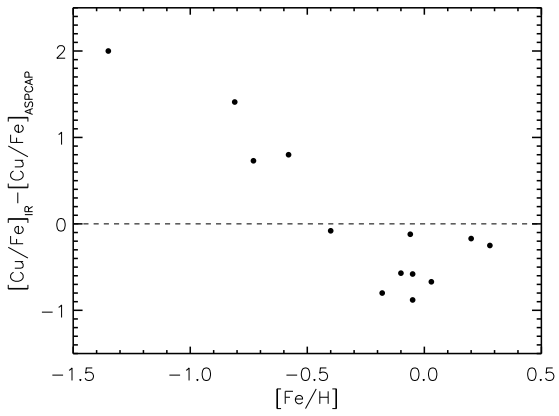

Fig. 5 Differences between the Cu abundances derived by our work and the ASPCAP for the sample stars.

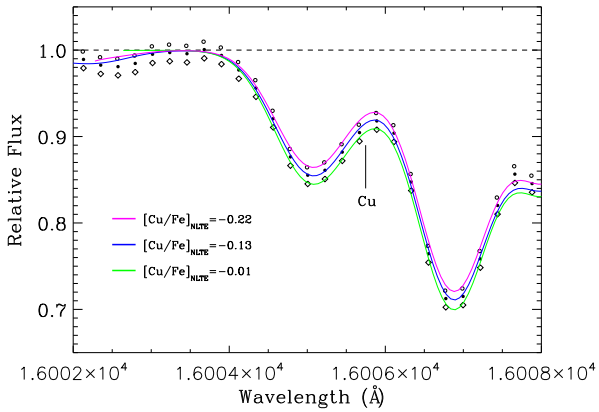

Fig. 6 Synthetic profiles of the Cu I 16005 Å line for HD 67447. The *filled circles* are the observational data; the *open diamonds* and *circles* are the observational data with an about 1% shift up and down of the continuum, respectively. The *blue*, *pink* and *green solid lines* are the best-fit NLTE synthesis.

the Arcturus at the APOGEE resolution, and display the profiles of each individual blending line, which were computed with the same external broadening profile as that for the synthetic spectrum. Obviously, the Cu I λ16005.748 line blends with the adjacent lines (i.e., C I, Ti II and Fe I). To investigate the effects of these lines on our [Cu/Fe] values, we tested to make the abundances of C, Ti and Fe, respectively, have a variation of 0.1 dex and checked how much our copper abundances varied. The results are listed in the last six columns of Table A1. It is noted that C I and Ti II lines have small influence, while Fe I lines show relatively important effects on the abundance derivation, which can be 0.15 dex.

In addition, the different adopted stellar parameters could partly lead to the discrepancy. Taking the star

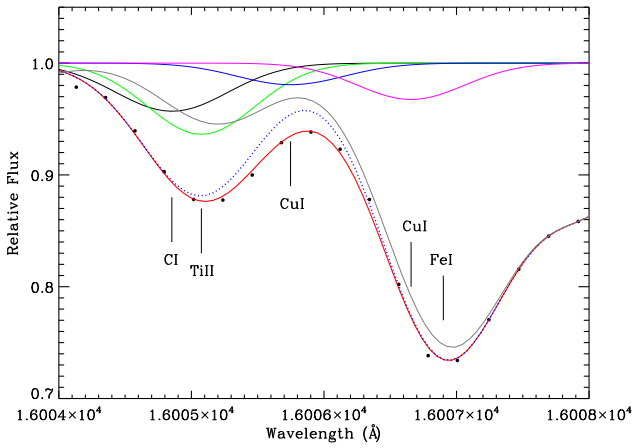

Fig. 7 Synthetic profiles of Cu I line at 16005.7 Å for the Arcturus at the APOGEE resolution. The *filled black circles* are the observation, the *red solid line* is the synthesis with Cu and the *blue dotted line* is the synthesis without the Cu line. Besides, the *black*, *green*, *blue*, *pink*, and *gray solid lines* respectively represent the synthetic profiles of each individual line, that is C I, Ti II, Cu I 16005 Å, Cu I 16006 Å, and Fe I, which are computed with the same external broadening profile as that for the synthetic spectrum.

HD 67447 for example, its stellar parameters are $T_{\rm eff}$ = 4933 K, $\log g$ = 2.17 dex, [Fe/H] = –0.05 dex, and ξ = 2.12 km s^{-1} for this work, while they are $T_{\rm eff}$ = 5023 K, $\log g$ = 2.78 dex, [Fe/H] = 0.06 dex, and ξ = 0.32 km s^{-1} for the ASPCAP. When we derived the copper abundance with the latter parameters, the obtained [Cu/Fe] value is –0.24 dex, which is lower than our result (–0.13 dex), and the difference is 0.11 dex. ASPCAP derives the stellar parameters with the code FERRE (Allende Prieto et al. 2006) and the raw parameters are used to derive the copper abundances. To investigate its impact on [Cu/Fe] ratios, we determined the copper abundances using the same parameters with ASPCAP in our analysis, and find about 0.1 dex differences of the derived results.

5.3.3 Comparison with previous work

As we know, only two groups have hitherto determined copper abundances for the APOGEE *H*-band spectra in LTE analysis. Only one star is in common with their studies (Smith et al. 2013; Hawkins et al. 2016): Arcturus. Smith et al. (2013) derived a [Cu/Fe] ratio of –0.23 dex for the Arcturus, which is lower than our calculation (-0.1 dex). Since we note that their [Fe/H] is –0.18 dex higher than ours, the difference may due to the different stellar parameters adopted in each work. While Hawkins et al. (2016) found the [Cu/Fe] value was –0.37 dex, which is –0.27 dex lower than ours. As both works adopted similar stellar parameters, the difference

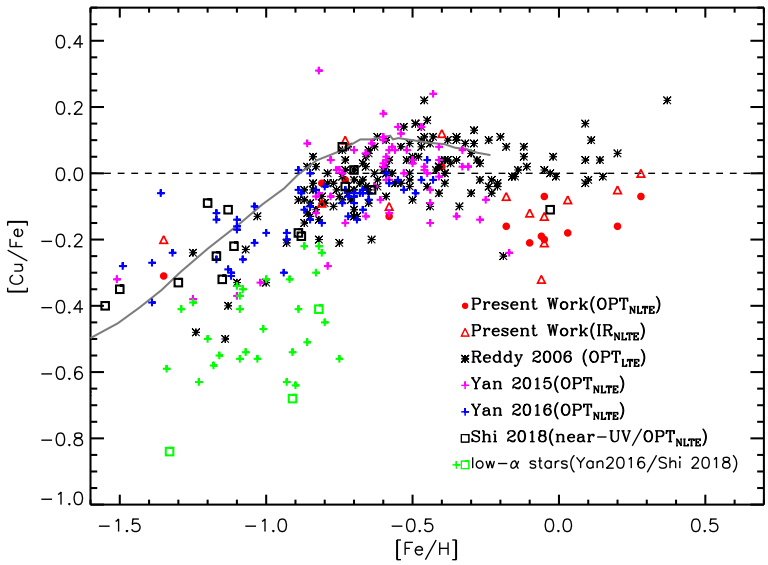

Fig. 8 [Cu/Fe] vs. [Fe/H] for the present sample (*red filled circles* for optical results and *red triangles* for IR results), Reddy et al. (2006, *black asterisks)*, Yan et al. (2015, *pink plus signs)*, Yan et al. (2016, *blue plus signs*, thick disk/high-α stars), Shi et al. (2018, *black squares*, disk/halo stars). Besides, the *green plus signs* and *green squares* respectively represent low-α stars for the work of Yan et al. (2016) and Shi et al. (2018). The theoretical predictions of Kobayashi et al. (2006, *grey solid line)* are also presented.

could be owing to the different $\log gf$ values of the Cu I line.

5.4 The Evolutionary Trend of [Cu/Fe] in the Galactic Disk

It is interesting to explore the behavior of [Cu/Fe] ratios on account of its importance on revealing the nature of Cu nucleosynthesis, and constraining the Galactic chemical evolution (GCE) model. In Figure 8, we present the [Cu/Fe] abundances versus [Fe/H] for our NLTE measurements (red filled circles for optical and red triangles for IR), together with the LTE results from Reddy et al. (2006, black asterisks), the NLTE results from Yan et al. (2015, pink plus signs), Yan et al. (2016, blue/green plus signs) and Shi et al. (2018, black/green squares). The green plus signs and squares represent low-α stars, which show systematic low copper abundances (Nissen & Schuster 2011; Yan et al. 2016). Except for the green symbols, there is a rather good agreement between our calculations with the previous results in the metallicity range of $\sim$–1.4 < [Fe/H] < $\sim$–0.2 dex, while a discrepancy exists when [Fe/H] > –0.2 dex: our [Cu/Fe] ratios are less enhanced than those from Reddy et al. (2006). We guess it could be ascribed to the paucity of sample stars in this region or the different adopted analysis methods. As the copper lines are heavily blended for metal-rich stars, it is essential to consider other blending lines in copper abundance studies, which may be one of the reasons for the discrepancy.

In Figure 8, several features of the [Cu/Fe] trend can be found: it seems to slightly decline with increasing [Fe/H] down to solar metallicity, it then increases with decreasing [Fe/H] in the metallicity range of $\sim$–0.5 < [Fe/H] < $\sim$0.0 dex, while it declines linearly with decreasing metallicity when [Fe/H] < $\sim$–0.5 dex. Although the exact origins of copper are complex (e.g., see Bisterzo et al. 2004, and references therein), the significant secondary (i.e., metallicity-dependent) production of Cu can be seen throughout the range $\sim$–1.4 < [Fe/H] < $\sim$–0.5 dex.

Many studies (e.g. Sneden et al. 1991; Timmes et al. 1995; Goswami & Prantzos 2000; Mishenina et al. 2002; Kobayashi et al. 2006, 2011; Romano & Matteucci 2007; Romano et al. 2010) have modeled the Galactic chemical evolution of copper. In Figure 8 we also display the results predicted by Kobayashi et al. (2006, grey solid line). It seems that our [Cu/Fe] ratios are consistent with their model predictions, showing a similar [Cu/Fe] trend with their results throughout the range $\sim$–1.4 < [Fe/H] < $\sim$–0.2 dex.

6 CONCLUSIONS

We wish to derive the reliable Cu abundances with the Cu I lines in the APOGEE *H*-band spectra, thus we explored the NLTE effects of the *H*-band Cu I lines, and also verified the reliability of our Cu atomic model. We measured the LTE

and NLTE copper abundances using the APOGEE *H*-band and optical spectra for 13 FGK stars. The conclusions can be summarized in the following points:

1. Our results show that the NLTE effects in IR Cu I line at 16005.7 Å are negligible, indicating that it forms under the LTE conditions.
2. When the uncertainties are taken into account, consistent abundances from the *H*-band and optical copper lines are derived. It suggests that our copper calculations are reliable and the Cu atomic model is valid for investigating the formation of the *H*-band Cu I lines.
3. The [Cu/Fe] ratios increase with increasing [Fe/H] when $\sim -1.4 <$ [Fe/H] $< \sim -0.5$ dex, which may indicate a secondary (metallicity-dependent) production of Cu.

This work is the first, where Cu abundances were obtained from the APOGEE *H*-band spectra and the NLTE effects in IR Cu I line at 16005 Å were investigated. Although the *H*-band Cu I line used for our investigation is blended with other lines, a consistent result between the optical and *H*-band lines can be obtained when the blending lines are considered. We obtain relatively reliable [Cu/Fe] values with the *H*-band Cu I lines, even though the NLTE effects are neglectable, and our calculations will be helpful to calibrate the ASPCAP results.

Acknowledgements This research is supported by the Key Research Program of the Chinese Academy of Sciences (Grant No. XDPB09-02) and the National Key Basic Research Program of China (Grant No. 2014CB845700), and the National Natural Science Foundation of China (Grant Nos. 11833006, 11473033, 11603037 and 11803049), and International partnership program's Key foreign cooperation project, Bureau of International Cooperation, Chinese Academy of Sciences (Grant No. 114A32KYSB20160049). This work is also supported by the Astronomical Big Data Joint Research Center, co-founded by the National Astronomical Observatories, Chinese Academy of Sciences and the Alibaba Cloud.

This work uses data from the Xinglong 2.16 m, ARC 3.5 m, Lijiang Observatory 1.8 m, and Calar Alto 2.2 m telescopes. We acknowledge the support of the staff at these telescopes. This work also uses data from the NOAO Science Archive, Kitt Peak Solar Atlas, and SDSS DR14. Funding for the Sloan Digital Sky Survey IV has been provided by the Alfred P. Sloan Foundation, the U.S. Department of Energy Office of Science, and the Participating Institutions. SDSS-IV acknowledges support and resources from the Center for High-Performance Computing at the University of Utah. The SDSS web site is www.sdss.org.

SDSS-IV is managed by the Astrophysical Research Consortium for the Participating Institutions of the SDSS Collaboration, including the Brazilian Participation Group, the Carnegie Institution for Science, Carnegie Mellon University, the Chilean Participation Group, the French Participation Group, Harvard-Smithsonian Center for Astrophysics, Instituto de Astrofísica de Canarias, The Johns Hopkins University, Kavli Institute for the Physics and Mathematics of the Universe (IPMU)/University of Tokyo, Lawrence Berkeley National Laboratory, Leibniz Institut für Astrophysik Potsdam (AIP), Max-Planck-Institut für Astronomie (MPIA Heidelberg), Max-Planck-Institut für Astrophysik (MPA Garching), Max-Planck-Institut für Extraterrestrische Physik (MPE), National Astronomical Observatories of China, New Mexico State University, New York University, University of Notre Dame, Observatório Nacional/MCTI, The Ohio State University, Pennsylvania State University, Shanghai Astronomical Observatory, United Kingdom Participation Group, Universidad Nacional Autónoma de México, University of Arizona, University of Colorado Boulder, University of Oxford, University of Portsmouth, University of Utah, University of Virginia, University of Washington, University of Wisconsin, Vanderbilt University, and Yale University.

Appendix A: ADDITIONAL TABLES

We provide three additional tables. The first table (Table A1) provides the values of [C/Fe] and [Ti/Fe] for our program stars. Both the abundances were derived based on optical lines with the spectral synthesis method. To get rid of the NLTE effects, we only selected the C and Ti lines that are not sensitive to the NLTE effects. The detailed information about the adopted C and Ti lines can be seen in Alexeeva & Mashonkina (2015) and Zhao et al. (2016). Besides, to investigate the effects of the blending lines on our [Cu/Fe] values, we made the abundances of C, Ti and Fe, respectively, have a variation of 0.1 dex and list the results in the last columns of Table A1. The second table (Table A2) gives the atomic data of the blending lines described in Section 3.1.2. The third table (Table A3) presents the LTE and NLTE Cu abundances derived from the individual optical lines. Details on these tables are given below.

Appendix B: ADDITIONAL FIGURES

We compare our C and Ti abundances with the results from Zhao et al. (2016).

Table A1 C, Ti Abundances and the Variation of [Cu/Fe] due to the Blending Lines

Star	[C/Fe]	[Ti/Fe]	Δ[Cu/Fe]$_{\rm C}$		Δ[Cu/Fe]$_{\rm Ti}$		Δ[Cu/Fe]$_{\rm Fe}$	
			+0.1	–0.1	+0.1	–0.1	+0.1	–0.1
Arcturus	0.26 ± 0.06	0.19 ± 0.05	–0.02	0.00	–0.04	0.00	–0.13	0.06
HD 87	–0.22 ± 0.03	0.00 ± 0.03	–0.02	0.00	–0.02	0.00	–0.08	0.05
HD 6582	0.16 ± 0.02	0.23 ± 0.04	–0.02	0.03	–0.01	0.02	–0.11	0.13
HD 6920	–0.04 ± 0.02	0.00 ± 0.04	–0.04	0.02	–0.04	0.00	–0.13	0.12
HD 22675	–0.22 ± 0.04	–0.01± 0.02	–0.02	0.03	0.00	0.02	–0.12	0.13
HD 58367	–0.22 ± 0.02	–0.03 ± 0.05	0.00	0.01	–0.01	0.02	–0.07	0.07
HD 67447	–0.16 ± 0.03	–0.08 ± 0.03	–0.02	0.00	–0.03	0.00	–0.12	0.07
HD 102870	–0.08 ± 0.03	–0.09 ± 0.01	0.00	0.00	0.00	0.02	–0.11	0.10
HD 103095	–0.15 ± 0.00	0.27 ± 0.03	0.00	0.00	–0.03	0.03	–0.15	0.14
HD 121370	–0.01 ±0.04	0.12 ± 0.03	–0.05	0.03	–0.03	0.03	–0.13	0.10
HD 148816	0.20 ± 0.00	0.24 ± 0.04	–0.08	0.05	–0.06	0.04	–0.15	0.14

Table A2 Atomic Data of Other Blending Lines

Ion	λ_{air} (Å)	$E_{\rm low}$ (eV)	$\log gf$	$\log C_6$
C I	16004.853	9.631	0.104	–32.000
Ti II	16005.075	3.095	–2.234	–32.040
Fe I	16005.170	6.222	–0.580	–30.545
Fe I	16005.383	2.865	–5.620	–31.870
Cu I	16005.748	5.348	–0.018	–32.000
Fe I	16006.178	3.368	–5.400	–31.820
Fe I	16006.633	2.865	–5.100	–31.870
Cu I	16006.657	5.348	0.500	–32.000
Fe I	16006.800	6.347	0.557	–30.620
Fe I	16007.106	6.347	–0.060	–30.645
Fe I	16007.383	2.865	–4.630	–31.870
Fe I	16008.080	6.266	0.095	–30.620

Table A3 [Cu/Fe] based on Optical Cu I Lines under LTE and NLTE Analyses

	5105 (Å)		5218 (Å)		5700 (Å)		5782 (Å)	
Star	LTE	NLTE	LTE	NLTE	LTE	NLTE	LTE	NLTE
Arcturus	–0.13	–0.10	–0.14	–0.15	···	···	···	···
HD 87	–0.28	–0.24	–0.23	–0.25	···	···	–0.19	–0.13
HD 6582	–0.04	+0.02	–0.12	–0.11	···	···	–0.05	+0.00
HD 6920	–0.24	–0.20	–0.26	–0.24	···	···	–0.17	–0.12
HD 22675	–0.14	–0.10	···	···	···	···	–0.10	–0.04
HD 31501	+0.02	+0.04	+0.02	+0.02	+0.00	+0.02	+0.00	+0.02
HD 58367	–0.27	–0.18	···	···	–0.26	–0.19	–0.20	–0.10
HD 67447	–0.27	–0.21	···	···	–0.26	–0.21	–0.25	–0.18
HD 102870	–0.15	–0.14	–0.20	–0.21	···	···	–0.16	–0.14
HD 103095	–0.27	–0.21	–0.38	–0.37	···	···	–0.39	–0.34
HD 121370	–0.09	–0.08	–0.06	–0.08	–0.05	–0.04	···	···
HD 148816	–0.08	+0.02	–0.14	–0.08	···	···	–0.09	+0.01
HD 177249	–0.12	–0.19	–0.21	–0.23	–0.24	–0.20	–0.16	–0.11

References

Abolfathi, B., Aguado, D. S., Aguilar, G., et al. 2018, ApJS, 235, 42

Allen, C. W. 1973, Astrophysical Quantities (London: University of London, Athlone Press, —c1973, 3rd ed.)

Alexeeva, S. A., & Mashonkina, L. I. 2015, MNRAS, 453, 1619

Allende Prieto, C., Beers, T. C., Wilhelm, R., et al. 2006, ApJ, 636, 804

Andrievsky, S., Bonifacio, P., Caffau, E., et al. 2018, MNRAS, 473, 3377

Anstee, S. D., & O'Mara, B. J. 1991, MNRAS, 253, 549

Anstee, S. D., & O'Mara, B. J. 1995, MNRAS, 276, 859

Arlandini, C., Käppeler, F., Wisshak, K., et al. 1999, ApJ, 525, 886

Asplund, M., Grevesse, N., Sauval, A. J., & Scott, P. 2009, ARA&A, 47, 481

Biehl, D. 1976, PhD thesis, University of Kiel

Bihain, G., Israelian, G., Rebolo, R., et al. 2004, A&A, 423, 777

Bisterzo, S., Gallino, R., Pignatari, M., et al. 2004, Mem. Soc. Astron. Italiana, 75, 741

Butler, K., & Giddings, J. R. 1985, Newsletter on the Analysis of Astronomical Spectra, 9 (London: Univ. London)

Cowan, J. J., Sneden, C., Burles, S., et al. 2002, ApJ, 572, 861

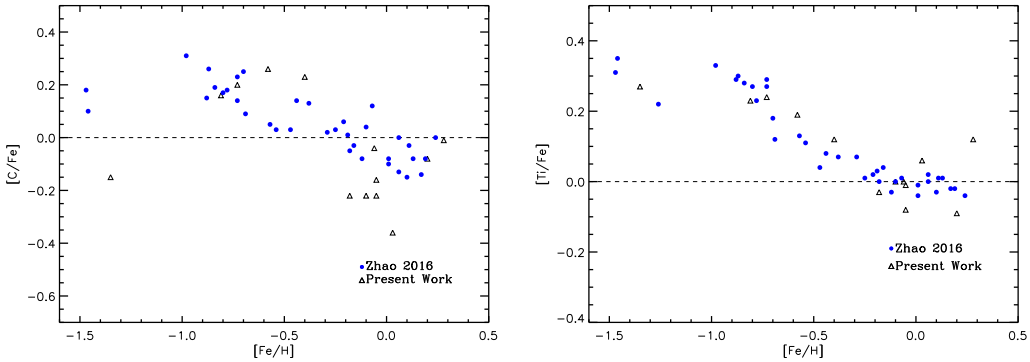

Fig. B.1 Comparisons of C and Ti abundances between our work and Zhao et al. (2016).

Drawin, H.-W. 1968, Zeitschrift für Physik, 211, 404
Drawin, H. W. 1969, Zeitschrift fur Physik, 225, 483
Eisenstein, D. J., Weinberg, D. H., Agol, E., et al. 2011, AJ, 142, 72
Fink, M., Kromer, M., Seitenzahl, I. R., et al. 2014, MNRAS, 438, 1762
García Pérez, A. E., Allende Prieto, C., Holtzman, J. A., et al. 2016, AJ, 151, 144
Goswami, A., & Prantzos, N. 2000, A&A, 359, 191
Gratton, R. G., & Sneden, C. 1988, A&A, 204, 193
Gustafsson, B., Edvardsson, B., Eriksson, K., et al. 2008, A&A, 486, 951
Hawkins, K., Masseron, T., Jofré, P., et al. 2016, A&A, 594, A43
Hinkle, K., Wallace, L., & Livingston, W. 1995, PASP, 107, 1042
Holtzman, J. A., Shetrone, M., Johnson, J. A., et al. 2015, AJ, 150, 148
Holtzman, J. A., Hasselquist, S., Shetrone, M., et al. 2018, AJ, 156, 125
Ishigaki, M. N., Aoki, W., & Chiba, M. 2013, ApJ, 771, 67
Iwamoto, K., Brachwitz, F., Nomoto, K., et al. 1999, ApJS, 125, 439
Jönsson, H., Allende Prieto, C., Holtzman, J. A., et al. 2018, AJ, 156, 126
Kobayashi, C., Umeda, H., Nomoto, K., et al. 2006, ApJ, 653, 1145
Kobayashi, C., Karakas, A. I., & Umeda, H. 2011, MNRAS, 414, 3231
Kurucz, R. L., Furenlid, I., Brault, J., & Testerman, L. 1984, Solar Flux Atlas from 296 to 1300 nm (National Solar Observatory Atlas, Sunspot, New Mexico: National Solar Observatory)
Lai, D. K., Bolte, M., Johnson, J. A., et al. 2008, ApJ, 681, 1524
Limongi, M., & Chieffi, A. 2003, ApJ, 592, 404
Liu, Y. P., Gao, C., Zeng, J. L., et al. 2014, ApJS, 211, 30
Majewski, S. R., Schiavon, R. P., Frinchaboy, P. M., et al. 2017, AJ, 154, 94
Matteucci, F., Raiteri, C. M., Busson, M., et al. 1993, A&A, 272, 421
Mishenina, T. V., Kovtyukh, V. V., Soubiran, C., et al. 2002, A&A, 396, 189
Nissen, P. E., & Schuster, W. J. 2011, A&A, 530, A15
Pignatari, M., Gallino, R., Heil, M., et al. 2010, ApJ, 710, 1557
Reddy, B. E., Tomkin, J., Lambert, D. L., et al. 2003, MNRAS, 340, 304
Reddy, B. E., Lambert, D. L., & Allende Prieto, C. 2006, MNRAS, 367, 1329
Reetz, J. K. 1991, Diploma thesis, Universität München
Romano, D., & Matteucci, F. 2007, MNRAS, 378, L59
Romano, D., Karakas, A. I., Tosi, M., & Matteucci, F. 2010, A&A, 522, A32
Rybicki, G. B., & Hummer, D. G. 1991, A&A, 245, 171
Rybicki, G. B., & Hummer, D. G. 1992, A&A, 262, 209
Seaton, M. J. 1962, in Atomic and Molecular Processes, ed. D. R. Bates, 375
Shi, J. R., Gehren, T., Zeng, J. L., et al. 2014, ApJ, 782, 80
Shi, J. R., Yan, H. L., Zhou, Z. M., et al. 2018, ApJ, 862, 71
Simmerer, J., Sneden, C., Ivans, I. I., et al. 2003, AJ, 125, 2018
Smith, V. V., Cunha, K., Shetrone, M. D., et al. 2013, ApJ, 765, 16
Sneden, C., & Crocker, D. A. 1988, ApJ, 335, 406
Sneden, C., Gratton, R. G., & Crocker, D. A. 1991, A&A, 246, 354
Sneden, C., Cowan, J. J., Lawler, J. E., et al. 2003, ApJ, 591, 936
Steenbock, W., & Holweger, H. 1984, A&A, 130, 319
Timmes, F. X., Woosley, S. E., & Weaver, T. A. 1995, ApJS, 98, 617
Travaglio, C., Hillebrandt, W., Reinecke, M., et al. 2004, A&A, 425, 1029
van Regemorter, H. 1962, ApJ, 136, 906
Westin, J., Sneden, C., Gustafsson, B., et al. 2000, ApJ, 530, 783
Woosley, S. E., & Weaver, T. A. 1995, ApJS, 101, 181
Xu, X. D., Shi, J. R., & Yan, H. L. 2019, ApJ, 875, 142
Yan, H. L., Shi, J. R., Nissen, P. E., et al. 2016, A&A, 585, A102
Yan, H. L., Shi, J. R., & Zhao, G. 2015, ApJ, 802, 36
Zhang, J., Shi, J., Pan, K., et al. 2016, ApJ, 833, 137
Zhang, J., Shi, J., Pan, K., et al. 2017, ApJ, 835, 90
Zhao, G., Mashonkina, L., Yan, H. L., et al. 2016, ApJ, 833, 225
Zhou, Z.-M., Pan, K., Shi, J.-R., et al. 2019, ApJ, 881, 77